Check for updates

VIP Zn-I_2 Batteries Very Important Paper

How to cite:
International Edition: doi.org/10.1002/anie.202303011
German Edition: doi.org/10.1002/ange.202303011

Organic pH Buffer for Dendrite-Free and Shuttle-Free Zn-I_2 Batteries

Yanqiu Lyu, Jodie A. Yuwono, Pengtang Wang, Yanyan Wang, Fuhua Yang, Sailin Liu, Shilin Zhang, Baofeng Wang, Kenneth Davey, Jianfeng Mao, and Zaiping Guo**

Abstract: Aqueous Zn-Iodine (I_2) batteries are attractive for large-scale energy storage. However, drawbacks include, Zn dendrites, hydrogen evolution reaction (HER), corrosion and, cathode "shuttle" of polyiodines. Here we report a class of N-containing heterocyclic compounds as organic pH buffers to obviate these. We evidence that addition of pyridine /imidazole regulates electrolyte pH, and inhibits HER and anode corrosion. In addition, pyridine and imidazole preferentially absorb on Zn metal, regulating non-dendritic Zn plating /stripping, and achieving a high Coulombic efficiency of 99.6 % and long-term cycling stability of 3200 h at 2 mA cm^{-2}, 2 mAh cm^{-2}. It is also confirmed that pyridine inhibits polyiodines shuttling and boosts conversion kinetics for I^-/I_2. As a result, the Zn-I_2 full battery exhibits long cycle stability of $>25\,000$ cycles and high specific capacity of 105.5 mAh g^{-1} at 10 A g^{-1}. We conclude organic pH buffer engineering is practical for dendrite-free and shuttle-free Zn-I_2 batteries.

Introduction

Emerging climate change has meant an increasing global commitment to carbon neutrality within the next few decades. Rapid adoption of clean energy is important to reduce carbon emissions. Because of intermittence of clean energy including, solar and wind, development of reliable energy storage beyond conventional lithium-ion batteries is needed.[1] Aqueous, rechargeable zinc batteries are emerging as practically promising for grid-scale energy storage owing to high capacity of Zn of 820 mAh g^{-1}, low cost, high safety and eco-friendliness.[2] Amongst cathode materials, iodine is attractive because of high specific capacity of 221 mAh g_{iodine}^{-1}, high discharge potential plateau of 1.38 V vs. Zn/Zn^{2+} and abundance in seawater at 55 μg L^{-1}. As a result, aqueous zinc-iodine (Zn-I_2) batteries have attracted research attention for energy storage.[3] However drawbacks include, for the anode, Zn metal exhibits dendrite growth and thermodynamics favour HER.[4] For the cathode, high concentration of polyiodine intermediate compounds are generated during conversion of I_2/I^- that cause "shuttle" effects, leading to irreversible loss of active materials and corrosion and consumption of Zn anode.

Electrolyte optimization is an acknowledged practical means for suppression of Zn dendrites and HER because of facile preparation processes and low costs. For example, electrolyte additives, high concentration electrolytes and polymer gel electrolytes have been reported to suppress HER and boost plating/stripping reversibility of Zn.[4c,5] However, the influence of pH stability of electrolyte on H_2 evolution and dendrite formation in Zn batteries has been overlooked. The pH for many reported mild, aqueous Zn electrolytes is ca. 4, leading to HER and concentration increase in OH^- and formation of alkaline zincate ($Zn_xSO_y(OH)_z{\cdot}nH_2O$). Formation of alkaline zincate consumes Zn^{2+} and is a physical barrier affecting uniform Zn ion flux and facilitating Zn dendrite growth, underscoring the need to stabilize the pH during cycling. In addition, for continued development of Zn-I_2 full battery, the shuttle effect of polyiodine intermediate compounds also needs solution. Formation of polyiodine intermediates represented by I_3^- and reactions involved in Zn-I_2 battery can be described as follows:[6]

$$I^- + I_2 \rightarrow I_3^- \quad (1)$$

$$I_3^- + 2e^- \rightarrow 3I^- \quad (2)$$

$$Zn - 2e^- \rightarrow Zn^{2+} \quad (3)$$

High concentration of I_3^- diffuses to the Zn anode, leading to self-discharge and consuming Zn metal. At the same time, regenerated I^- reacts continuously with I_2 and converts to I_3^-, that consumes I_2 and affects the capacity decay of Zn-I_2 battery. By design therefore, a pH buffer electrolyte that concurrently regulates pH, protects Zn anode from corrosion, guides Zn uniform deposition and

[*] Y. Lyu, Dr. J. A. Yuwono, Dr. P. Wang, Y. Wang, Dr. F. Yang, Dr. S. Liu, Dr. S. Zhang, Prof. K. Davey, Dr. J. Mao, Prof. Z. Guo
School of Chemical Engineering, the University of Adelaide
Adelaide, SA 5005 (Australia)
E-mail: jianfeng.mao@adelaide.edu.au
zaiping.guo@adelaide.edu.au
Prof. B. Wang
Shanghai Key Laboratory of Materials Protection and Advanced Materials in Electric Power, Shanghai University of Electric Power
Shanghai, 200090 (China)

© 2023 The Authors. Angewandte Chemie International Edition published by Wiley-VCH GmbH. This is an open access article under the terms of the Creative Commons Attribution Non-Commercial License, which permits use, distribution and reproduction in any medium, provided the original work is properly cited and is not used for commercial purposes.

© 2023 The Authors. Angewandte Chemie International Edition published by Wiley-VCH GmbH

inhibits the shuttle of polyiodine compounds is needed for Zn-I_2 batteries.

Biological buffers based on organic substances are used in biochemical processes to maintain a constant pH over a given range *via* neutralizing effects of hydrogen ions. These keep pH constant by taking up protons that are released during reactions, or by releasing protons when they are consumed by reactions. It was hypothesized therefore that organic pH buffer molecules could be used as additives in aqueous electrolyte(s). In particular organic molecules that have N-containing groups serving as both acceptor and donor of hydrogen bonds. The amine /imine groups interact with Zn^{2+} and iodine, regulating Zn deposition and inhibiting the shuttle effect.[7] It was hypothesized that pH, Zn dendrites and shuttle effect in Zn-I_2 batteries could be concurrently controlled.

To test the hypothesis, initially, pyridine was added to 2 M $ZnSO_4$ electrolyte as an organic pH buffer. The unique lone pair on N forms a hydrogen bond with H, buffering pH change around Zn anode and inhibiting production of by-products. Pyridine molecules preferentially absorb on Zn metal surface and induce dendrite-free deposition of Zn (002) facet. Imidazole pH buffer that also contains N atoms, additionally, was used as an additive in 2 M $ZnSO_4$ electrolyte. The effect of organic pH buffer on reversibility and stability of Zn anode was demonstrated *via* electrochemical performance of Zn/Zn symmetrical cells tested at different current density and capacity, in 1) pyridine-$ZnSO_4$ electrolyte with 4000 h at 1 mA cm^{-2}, 1 mAh cm^{-2} and 3200 h at 2 mA cm^{-2}, 2 mAh cm^{-2}, and; 2) imidazole-$ZnSO_4$ electrolyte with 4000 h at 1 mA cm^{-2}, 1 mAh cm^{-2} and 800 h at 2 mA cm^{-2}, 2 mAh cm^{-2}. *In-situ* UV/Vis and *in-situ* Raman evidenced that the inhibition of polyiodides dissolution and high reversibility of I_2/I^- conversion in pyridine-$ZnSO_4$ electrolyte. As a result, Zn-I_2 batteries in pyridine-$ZnSO_4$ exhibited a high specific capacity of 180 mAh g^{-1} and ≈100 % Coulombic efficiency (CE) at 0.2 A g^{-1}, and reached 92 % capacity retention rate following 10000 cycles at a current density 2 A g^{-1}. At a high current density of 10 A g^{-1}, Zn-I_2 batteries in pyridine-$ZnSO_4$ reached 25000 cycles and maintained a high specific capacity of 105 mAh g^{-1}. It is concluded therefore that targeted engineering of electrolyte pH using organic buffer additive is of practical benefit in design for highly reversible and dendrite-free and shuttle-free Zn-I_2 batteries, and findings will be of interest to researchers and manufacturers.

Results and Discussion

The addition of pyridine or imidazole did not change the solvated structure of Zn^{2+} as was confirmed *via* FTIR (Figure S1) and Raman (Figure S2) spectra. The possible complex formed by imidazole and pyridine in acidic solution is highlighted in Figure S3. Imidazolium/imidazole and pyridinium/pyridine are conjugated acids / bases that can be used as buffers to regulate change of pH in electrolyte. When significant H^+ is produced in the electrolyte, imidazole and pyridine combine with H^+ to form imidazolium/ pyridinium. However, when H^+ in acid solution is consumed significant OH^- will combine with imidazolium/ pyridinium to form imidazole/pyridine. This reversible formation of pyridine/pyridinium and imidazole/imidazolium was confirmed *via* FTIR findings (Figures S4, S5). Because the concentration of pyridine and imidazole in $ZnSO_4$ electrolytes was significantly low, specific bands were not detected in FTIR. Therefore, 2 M H_2SO_4 was added to pyridine and imidazole-based electrolytes to determine the influence of acid on pyridine and imidazole. The vibration frequency for ring-breathing in liquid pyridine (vCC=N) is from 1700 to 1400 cm^{-1}, in which 1580 and 1481 cm^{-1} peak is (largely) affected by nitrogen lone pair (Figure S4).[8] When pyridine interacts with acid, the 1580 and 1481 cm^{-1} bands shift to high frequency and are stretched, evidencing that the nitrogen lone pairs of pyridine interact with H^+ under acidic condition. Similarly, in the imidazole ring structure of 1620 to 1500 cm^{-1}, the C=N peak at 1575 cm^{-1} blue-shifted significantly with addition of H_2SO_4 and C=C band was stretched and red-shifted, confirming the interaction of nitrogen lone pair and H^+ in imidazole (Figure S5).[9] To determine the adjustment effect of addition of imidazole and pyridine on pH of $ZnSO_4$ electrolyte, a home-made *in-situ* pH instrument was constructed to monitor pH change of the Zn anode in real-time (Figure S6). The pH meter was fixed in the home-made *in-situ* electrolytic cell with 50 mL electrolyte as close as practically possible to the Zn anode, in order to detect actual and accurate pH change of the Zn anode. The pyridine-$ZnSO_4$ and imidazole-$ZnSO_4$ had a positive change in pH. The initial pH in pyridine-$ZnSO_4$ and imidazole-$ZnSO_4$ were greater than that for 2 M $ZnSO_4$ electrolyte, with imidazole, 5.47 > 4.42 and pyridine, 5.5 > 4.42. Some imidazole/pyridine molecules combine with H^+ in the acidic electrolyte, resulting in an increase of pH of the electrolyte. Compared with mildly acidic electrolyte, the near-neutral aqueous electrolyte is a more benign solution environment for Zn metal anode.[10] The pH of the 2 M $ZnSO_4$ electrolyte without additives increased from 4.42 to 4.95 in discharge of the Zn/Zn symmetric battery, and decreased slightly during charge, and settled to maintain 4.86. However, the pH of 2 M $ZnSO_4$ electrolyte with imidazole, or pyridine, did not change significantly in both discharge and charge, Figure 1a (Figure S7, Table S1). For 2 M $ZnSO_4$ electrolyte, the change in pH near Zn anode during discharge is attributed to the fact of HER and a number of OH^- gathered to Zn anode, resulting in an increase in pH of Zn anode. In charging, because of conversion of current, the moving direction of cation and anion in the solution changes, leading to a drop in pH of Zn anode. However, for the pyridine-$ZnSO_4$ and imidazole-$ZnSO_4$ electrolyte, imidazolium, or pyridinium combine with generated OH^- and control growth of pH at Zn anode, and therefore suppress HER during discharge. Similarly, during charge the pH for Zn anode does not decrease, which is because of combination of imidazole/pyridine molecules and H^+ in the electrolyte. Therefore, addition of imidazole/ pyridine adjusts the pH of $ZnSO_4$ electrolyte in charge and discharge. To confirm inhibition of HER by additives, Linear Sweep Voltammetry (LSV) measurement was deter-

© 2023 The Authors. Angewandte Chemie International Edition published by Wiley-VCH GmbH

15213773, 0, Downloaded from https://onlinelibrary.wiley.com/doi/10.1002/anie.202303011 by University of Adelaide Alumni, Wiley Online Library on [26/04/2023]. See the Terms and Conditions (https://onlinelibrary.wiley.com/terms-and-conditions) on Wiley Online Library for rules of use; OA articles are governed by the applicable Creative Commons License

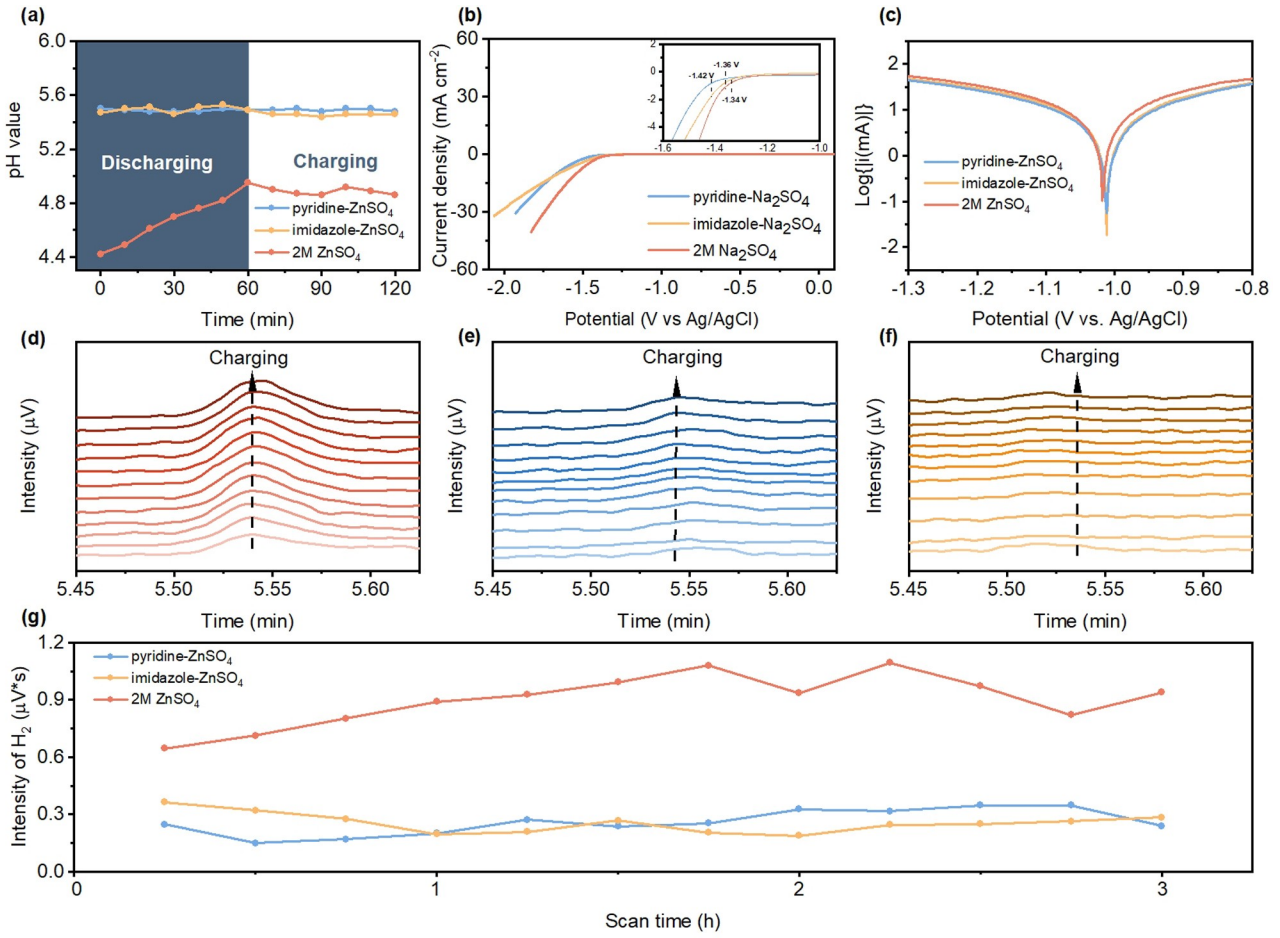

Figure 1. pH buffer and suppression of hydrogen evolution. a) Real-time electrolyte pH near Zn anode during discharge and charge at a current density of 1 mA cm^{-2}. b) Linear sweep voltammetry curves in pyridine-Na_2SO_4, imidazole- Na_2SO_4 and 2 M Na_2SO_4 electrolyte at a scan rate of 1 mV s^{-1}. c) Tafel plots for Zn plate tested in pyridine-$ZnSO_4$, imidazole-$ZnSO_4$ and 2 M $ZnSO_4$ electrolyte at a scan rate of 1 mV s^{-1}. d)–f) *In-situ* GC profile during Zn plating at 1 mA cm^{-2} (from (d) to (f): $ZnSO_4$, pyridine-$ZnSO_4$, imidazole-$ZnSO_4$). g) Corresponding H_2 release.

mined on different electrolytes. Because it is difficult to observe Zn deposition and H_2 release in the Zn–Ion electrolyte at similar potentials, 2 M Na_2SO_4 was used to replace 2 M $ZnSO_4$ to eliminate influence of Zn deposition on H_2 evolution.[11] 2 M Na_2SO_4 electrolyte exhibited HER response at −1.34 V vs. Ag/AgCl. In adding imidazole or pyridine, the potential response moved negatively, respectively, by 20 mV to −1.36 V vs. Ag/AgCl and by 80 mV to −1.42 V vs. Ag/AgCl confirming that additives significantly inhibit HER, Figure 1b. Tafel plot was used to determine the effect of electrolyte additives on Zn anode corrosion, Figure 1c. Compared with 2 M $ZnSO_4$ electrolyte, the corrosion potential for Zn in pyridine-$ZnSO_4$ electrolyte increased from −1.0179 to −1.0115 V, and; corrosion potential for Zn in imidazole-$ZnSO_4$ electrolyte increased from −1.0179 to −1.0120 V. In comparison with the corrosion current with 2 M $ZnSO_4$ (9.1 mA cm^{-2}) electrolyte on Zn, the corrosion current for pyridine-$ZnSO_4$ (4.66 mA cm^{-2}) and imidazole-$ZnSO_4$ (4.31 mA cm^{-2}) electrolyte on Zn decreased by, respectively, 4.44 and 4.79 mA cm^{-2}. It is generally acknowledged that the more positive the corrosion potential moves, the smaller the corrosion reaction for Zn and, the smaller the corrosion current, the lower the corrosion rate for Zn.[12] *In-situ* gas chromatography (GC) was used to determine release of H_2 (Figure S8). As is shown in Figures 1d–f, H_2 evolution is significantly inhibited by addition of imidazole and pyridine in 2 M $ZnSO_4$. H_2 was computed to estimate the impact of imidazole and pyridine on HER, Figure 1g. During the initial scan, 2 M $ZnSO_4$ exhibited H_2 release of 0.644 μV s. Importantly, this is 2.6 times greater than H_2 release for pyridine-$ZnSO_4$ (0.247 μV s) and 1.8 times greater than H_2 release from imidazole- $ZnSO_4$ (0.364 μV s). In continuous plating, the difference between H_2 release from 2 M $ZnSO_4$ electrolyte, imidazole- $ZnSO_4$ and pyridine-$ZnSO_4$ is more apparent. With continuous growth in plating time, the 2 M $ZnSO_4$ electrolyte increased continuously before 2 h, reaching a maximum release of H_2 of 1.08 μV s and remained balanced in subsequent scanning from the eighth scan, and fluctuated between 0.9 to 1.1 μV s. The release of H_2 from imidazole-$ZnSO_4$ and pyridine-$ZnSO_4$ electrolyte during the 3 h of plating is significantly less than for 2 M $ZnSO_4$ electrolyte and kept relatively stable from fluctuations with, pyridine-$ZnSO_4$: 0.349 to 0.149 μV s; imidazole-$ZnSO_4$: 0.364

© 2023 The Authors. Angewandte Chemie International Edition published by Wiley-VCH GmbH

15213773, 0, Downloaded from https://onlinelibrary.wiley.com/doi/10.1002/anie.202303011 by University of Adelaide Alumni, Wiley Online Library on [26/04/2023]. See the Terms and Conditions (https://onlinelibrary.wiley.com/terms-and-conditions) on Wiley Online Library for rules of use; OA articles are governed by the applicable Creative Commons License

to 0.187 μVs. These findings of stable and low H_2 release confirm the inhibitory effect of pyridine and imidazole on HER. It is concluded therefore that addition of imidazole and pyridine are practical pH buffers that regulate change of pH in the electrolyte, and inhibit HER and corrosion through formation/release of N–H bonds.

In addition to regulating the pH of electrolyte and inhibiting HER, the organic pH additive pyridine or imidazole, also suppresses dendrite growth and induces uniform Zn deposition. The deposition morphology for Zn metal depends significantly on initial nucleation behaviour in the electrodeposition. To determine the nucleation potential of different electrolyte therefore, cyclic voltammetry (CV) test was used in a three-electrode configuration. As is seen in Figure 2a, when scanning in the positive direction, the potential at point D is called "cross potential", which is a typical characteristic of the nucleation. Point A/B/C where Zn^{2+} begins to be reduced on the electrode is the nucleation overpotential (NOP). Compared with 2 M $ZnSO_4$, the addition of imidazole increased NOP by 6 mV, whilst the addition of pyridine increased it by 28 mV. It is widely acknowledged that the greater the nucleation overpotential, the smaller the nuclear radius is and the smaller the grain-size for the deposited Zn. This leads a uniform deposition of Zn.[12] Therefore, compared with $ZnSO_4$, the addition of imidazole and pyridine has a positive effect on uniform deposition of Zn. To establish the effect of pyridine-$ZnSO_4$ and imidazole-$ZnSO_4$ electrolyte on Zn nucleation, chronoamperometry (CA) was used, Figure 2b. When −1.2 V overpotential was applied, the current response of the three electrolytes within 10 s is attributed to the initial nucleation of Zn. With increase in time, 2 M $ZnSO_4$ exhibited a continuous increase in current density within 300 s, which is attributed to expansion of Zn deposition area because of significant Zn diffusion and formation of dendrite(s). However, in imidazole-$ZnSO_4$ and pyridine-$ZnSO_4$, the current remained stable during subsequent plating because of the overlap of Zn growth centres especially in pyridine-$ZnSO_4$ where the current response became stable following 50 s. It can be reliably concluded therefore that dense and smooth Zn deposition is more readily achieved in pyridine-$ZnSO_4$ and imidazole-$ZnSO_4$ than with 2 M $ZnSO_4$. To

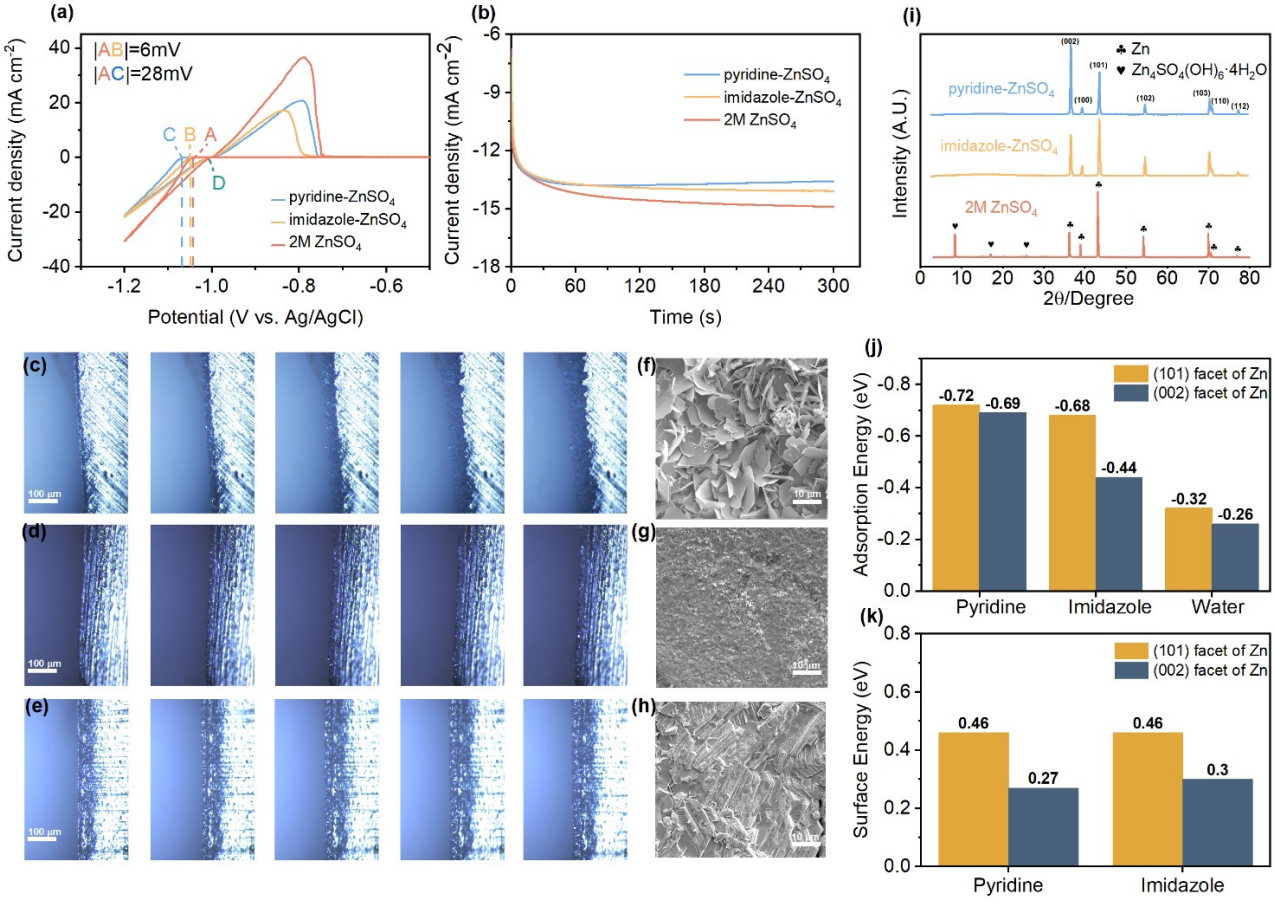

Figure 2. Regulation of Zn deposition and suppression of dendritic growth. a) Cyclic voltammograms (CVs) for Zn nucleation in pyridine-$ZnSO_4$, imidazole-$ZnSO_4$ and 2 M $ZnSO_4$. b) Chronoamperograms (CAs) for Zn metal in pyridine-$ZnSO_4$, imidazole-$ZnSO_4$ and 2 M $ZnSO_4$. *In-situ* optical microscopy of Zn plating at current density 2 mA cm^{-2} at 0, 5, 10, 15 and 20 min in c) 2 M $ZnSO_4$, d) imidazole-$ZnSO_4$ and e) pyridine-$ZnSO_4$. SEM image of Zn anode after cycled at 1 mA cm^{-2} in f) 2 M $ZnSO_4$, g) imidazole-$ZnSO_4$ and h) pyridine-$ZnSO_4$. i) XRD pattern for cycled Zn anode in 2 M $ZnSO_4$, pyridine-$ZnSO_4$ and imidazole-$ZnSO_4$. j) Computed adsorption energy for N atom in water, imidazole and pyridine on Zn (002) plane and Zn (101) plane. k) Computed surface energy for N atom in imidazole and pyridine on Zn (002) plane and Zn (101) plane.

© 2023 The Authors. Angewandte Chemie International Edition published by Wiley-VCH GmbH

15213773, 0, Downloaded from https://onlinelibrary.wiley.com/doi/10.1002/anie.202303011 by University of Adelaide Alumni, Wiley Online Library on [26/04/2023]. See the Terms and Conditions (https://onlinelibrary.wiley.com/terms-and-conditions) on Wiley Online Library for rules of use; OA articles are governed by the applicable Creative Commons License

confirm this, *in-situ* optical microscopic observations were undertaken view the deposition of Zn (Figure S9). As is shown in Figure 2c, for 2 M $ZnSO_4$ electrolyte, heterogeneous nucleation appeared in initial Zn deposition, and with the increase of time, Zn^{2+} were deposited around the site of the deposited Zn tip, resulting in growth of dendrites. However, for imidazole-$ZnSO_4$ and pyridine-$ZnSO_4$, deposition of Zn is relatively uniform, Figures 2d, e. During 20 min of electroplating, there was no apparent dendritic growth, evidencing that imidazole-$ZnSO_4$ and pyridine-$ZnSO_4$ are conducive to homogenization of nuclear sites and inhibit growth of dendrites. SEM was used to establish the difference in Zn deposition under different electrolyte. As shown in Figure 2f, Zn anode in 2 M $ZnSO_4$ exhibits irregular, clustered Zn deposition. However, in imidazole-$ZnSO_4$ and pyridine-$ZnSO_4$, the deposition of Zn is dense and uniform, especially in pyridine-$ZnSO_4$, with Zn exhibiting sheet-shape stacking in significant contrast to the irregular deposition for $ZnSO_4$, Figures 2g, h. At low magnification, it is more readily seen that irregular deposition of 2 M $ZnSO_4$ on Zn anode produces different deposition forms under the same electrode foil (Figure S10). X-Ray Diffraction (XRD) was used to determine corrosion on the Zn anode following 100 h cycling at 1 mA cm^{-2}, 1 mAh cm^{-2}, Figure 2i. XRD peaks of 8.5°, 17.1° and 25.8° were observed with 2 M $ZnSO_4$ electrolyte, that are attributed to by-products of $Zn_4SO_4(OH)_6{\cdot}4H_2O$ (PDF# 00-004-0673). The signal peaks for by-products are significantly weaker in pyridine-$ZnSO_4$ and imidazole-$ZnSO_4$, which evidences that imidazole and pyridine provide protection for Zn anode and inhibit accumulation of by-products. Additionally, the XRD findings evidenced that the Zn deposited on the pyridine-$ZnSO_4$ electrolyte at the peak of (002) at $2\theta = 36.2°$ is significantly stronger than (100), and more than (101) diffraction. This is not similar to the intensity of the diffraction peaks detected by 2 M $ZnSO_4$ and imidzole-$ZnSO_4$. The change in main peak intensity means that the differences in electrolyte affect the preferred orientation of Zn deposits, which is similar evidence from SEM findings. With N atoms in the additive, differing additive structures produce differing preferred orientations for Zn deposition. Density functional theory (DFT) computations were used to determine why imidazole and pyridine have different Zn deposition orientations with similar N heterocyclic compound structures. The preference for Zn facet deposition is closely related to adsorption energy and surface energy, Figures 2j, k. The adsorption of H_2O on the Zn slab, −0.26 eV in (002) or −0.32 eV in (101) facet, was found to be weaker than that for pyridine or imidazole, evidencing that pyridine or imidazole molecules are preferentially adsorbed on the surface of Zn so as to inhibit uncontrolled 2D diffusion and facilitate uniform and compact Zn deposition. This is evidenced in the SEM image, Figures 2f–h. Additionally, pyridine adsorption is stronger in (101) facet (−0.72 eV) compared with (002) facet (−0.69 eV). However, the effect on the surface energy with pyridine adsorption is found to be significantly stable in (002) facet (0.27 eV) than that in (101) facet (0.46 eV). Surface energy explains the stability of the surface, namely, the lower the value the more stable the surface configuration. This will give a dominant (002)-pyridine interaction.[13] The adsorption of imidazole is strong in (101) facet (−0.68 eV), much stronger than in (002) facet (−0.44 eV). However, the surface energy for imidazole-surface interaction expends significant surface energy for (101) facet (0.46 eV), therefore it is possible that there is imidazole-surface interaction in (002) because it has significantly lower surface energy (0.30 eV). Two peaks for imidazole/pyridine-surface interaction were observed in both (002) and (101) facet because of combination of surface energy and adsorption energy. However, the competing factor between these two needs to be considered. For pyridine-surface interaction, the dominant interaction is driven by the surface energy, whereas for imidazole-surface interaction, the dominant factor is adsorption energy. Compared with imidazole, pyridine is therefore more likely to induce Zn deposition orientation of Zn on (002) facet, as evidenced in experiment, Figure 2i.

Electrochemical performance, especially CE is an important parameter for electrolytes in commercial applications. Reversible plating/stripping testing of Zn was therefore used with Zn/Cu asymmetric batteries to determine reversibility of Zn in different electrolytes. As is seen in Figure 3a, the lower value CE in the first several cycles is because of reshaped Zn coordination.[14] CEs for 2 M $ZnSO_4$ are stable in the first 300 cycles (mean = 98.6 %), but decay rapidly in subsequent cycles because of formation of dendrites, or by-products. In contrast Zn/Cu batteries using pyridine-$ZnSO_4$ exhibit better CEs, and maintain a CE mean = 99.6 % for >1800 cycles. In imidazole-$ZnSO_4$, the mean CEs reached 99.4 %. Additionally, the increased mean CEs for pyridine-$ZnSO_4$ and imidazole-$ZnSO_4$ exhibit significantly better cycle reversibility, Figure 3b (Figure S11). The Zn/Zn symmetric battery was used to establish the effect of pyridine-$ZnSO_4$ and imidazole-$ZnSO_4$ on boosting the electrochemical stability of Zn longer-term (Figure S12). The voltage curve for Zn/Zn symmetrical battery exhibits irregular fluctuations after cycling for 450 h (1 mA cm^{-2}, 1 mAh cm^{-2}), and failed following 560 h in 2 M $ZnSO_4$ (Figure S13). In contrast, the regulation of pH and Zn deposition *via* electrolyte additive(s) in symmetrical batteries with pyridine-$ZnSO_4$ and imidazole-$ZnSO_4$ exhibited a stable cycling for >4000 h at 1 mA cm^{-2}, 1 mA cm^{-2}. To establish requirements for potential practical application and determine the effect of additives in electrolyte modification, the current density and capacity were gradually increased. Under test conditions of 2 mA cm^{-2} and 2 mAh cm^{-2}, the cycle stability for 2 M $ZnSO_4$ and modified electrolyte exhibited an apparent gap, Figure 3c. Zn/Zn symmetric battery circulated stably for just 200 h in 2 M $ZnSO_4$. In contrast, Zn/Zn symmetric battery circulated stably for 800 h in imidazole-$ZnSO_4$, and the cycle time for symmetric battery in pyridine-$ZnSO_4$ was 16 times than that for 2 M ZnSO4, reaching some 3200 h. The cycle time for Zn in pyridine-$ZnSO_4$ was significantly greater than that for imidazole-$ZnSO_4$, most likely because of the different orientation of Zn deposition, evidencing the superiority of Zn (002) facet deposition induced by pyridine-$ZnSO_4$, Figure 2i. Additionally, with high current density and high

© 2023 The Authors. Angewandte Chemie International Edition published by Wiley-VCH GmbH

15213773, 0, Downloaded from https://onlinelibrary.wiley.com/doi/10.1002/anie.202303011 by University of Adelaide Alumni, Wiley Online Library on [26/04/2023]. See the Terms and Conditions (https://onlinelibrary.wiley.com/terms-and-conditions) on Wiley Online Library for rules of use; OA articles are governed by the applicable Creative Commons License

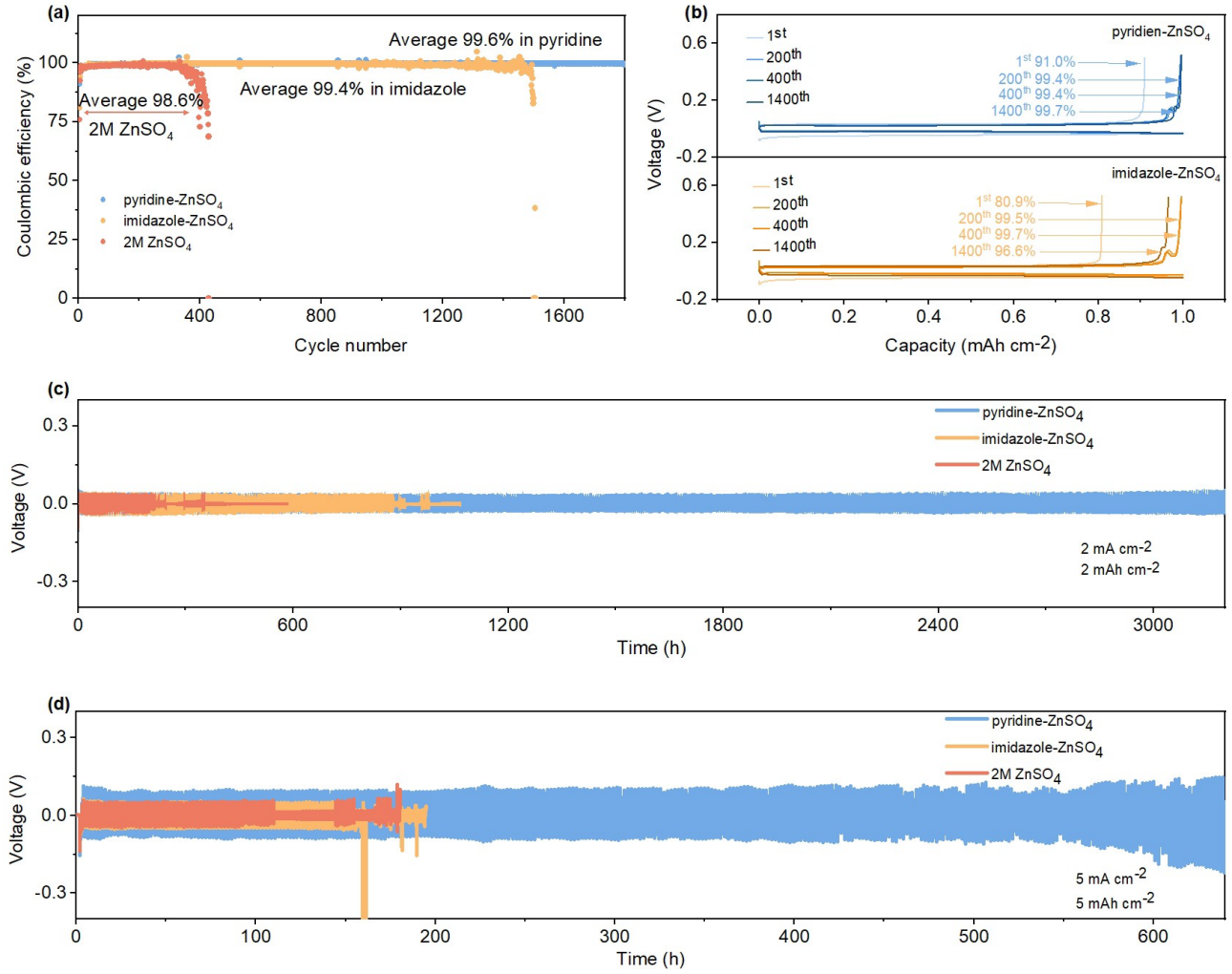

Figure 3. Zn plating/stripping on the selected electrolytes. a) Coulombic efficiency (CE) for Zn/Cu in 2 M $ZnSO_4$, pyridine-$ZnSO_4$ and imidazole-$ZnSO_4$. b) Corresponding voltage profile at selected cycles based on Zn/Cu in pyridine-$ZnSO_4$ and imidazole-$ZnSO_4$. Comparison of long-term galvanostatic charging/discharging of Zn/Zn symmetric cell in 2 M $ZnSO_4$, pyridine-$ZnSO_4$ and imidazole-$ZnSO_4$ at, respectively, current density and capacity of, c) 2 mA cm^{-2}, 2 mAh cm^{-2}, d) 5 mA cm^{-2}, 5 mAh cm^{-2}.

capacity of 5 mA cm^{-2} and 5 mAh cm^{-2}, the pyridine-$ZnSO_4$ supports the cycle of Zn/Zn symmetric battery for up to 600 h, which is significantly greater than for 2 M $ZnSO_4$ of 110 h and imidazole-$ZnSO_4$ of 155 h, Figure 3d. It is acknowledged that the electrolysis of H_2O in the electrolyte continues to intensify at high current density, accelerating change in pH for 2 M $ZnSO_4$ electrolyte. Coupled with the uneven deposition of Zn, this leads to a rapid short-circuit of Zn/Zn symmetric battery in 2 M $ZnSO_4$. However, because of the function of organic pH additives, Zn/Zn symmetric batteries exhibited superior stability despite 'harsh' test conditions, Table S2. It is concluded therefore these findings confirm the significant impact of organic pH buffer pyridine on stabilizing pH, inhibiting occurrence of by-products and in homogenizing Zn deposition.

Amongst aqueous Zn-ion batteries, Zn-I_2 full battery is practically attractive because of, resource abundance in seawater, high specific capacity and high discharge potential plateau.[3b] A full battery of Zn-I_2 was therefore assembled to demonstrate our organic pH buffer additives. As is shown in the CV curve, Figure 4a, there is one paired reduction and oxidation peaks in 2 M $ZnSO_4$, pyridine-$ZnSO_4$ and imidazole-$ZnSO_4$. Closer redox peak voltage and higher current make that pyridine-$ZnSO_4$ and imidazole-$ZnSO_4$ exhibit better electrochemical reaction kinetics and iodine utilization than 2 M $ZnSO_4$ electrolyte.[15] As presented in Figure 4b, the initial specific capacity for Zn-I_2 battery at 2 M $ZnSO_4$ is 152.4 mAh g^{-1} at current density 0.2 A g^{-1} that increased for a period reaching a maximum of 163.3 mAh g^{-1}, to decline in subsequent cycles. Following 400 cycles the capacity decayed to 144.4 mAh g^{-1}. In contrast the initial specific capacity for Zn-I_2 full battery in pyridine-$ZnSO_4$ is 165.8 mAh g^{-1}. Following, specific capacity increased to 180 mAh g^{-1}, and circulated stably under low current density to maintain a good charge/discharge. The initial specific capacity for Zn-I_2 full battery in imidazole-$ZnSO_4$ of 164.1 mAh g^{-1} was greater than that in 2 M $ZnSO_4$ and comparable to that in pyridine-$ZnSO_4$, however specific

© 2023 The Authors. Angewandte Chemie International Edition published by Wiley-VCH GmbH

15213773, 0, Downloaded from https://onlinelibrary.wiley.com/doi/10.1002/anie.202303011 by University of Adelaide Alumni, Wiley Online Library on [26/04/2023]. See the Terms and Conditions (https://onlinelibrary.wiley.com/terms-and-conditions) on Wiley Online Library for rules of use; OA articles are governed by the applicable Creative Commons License

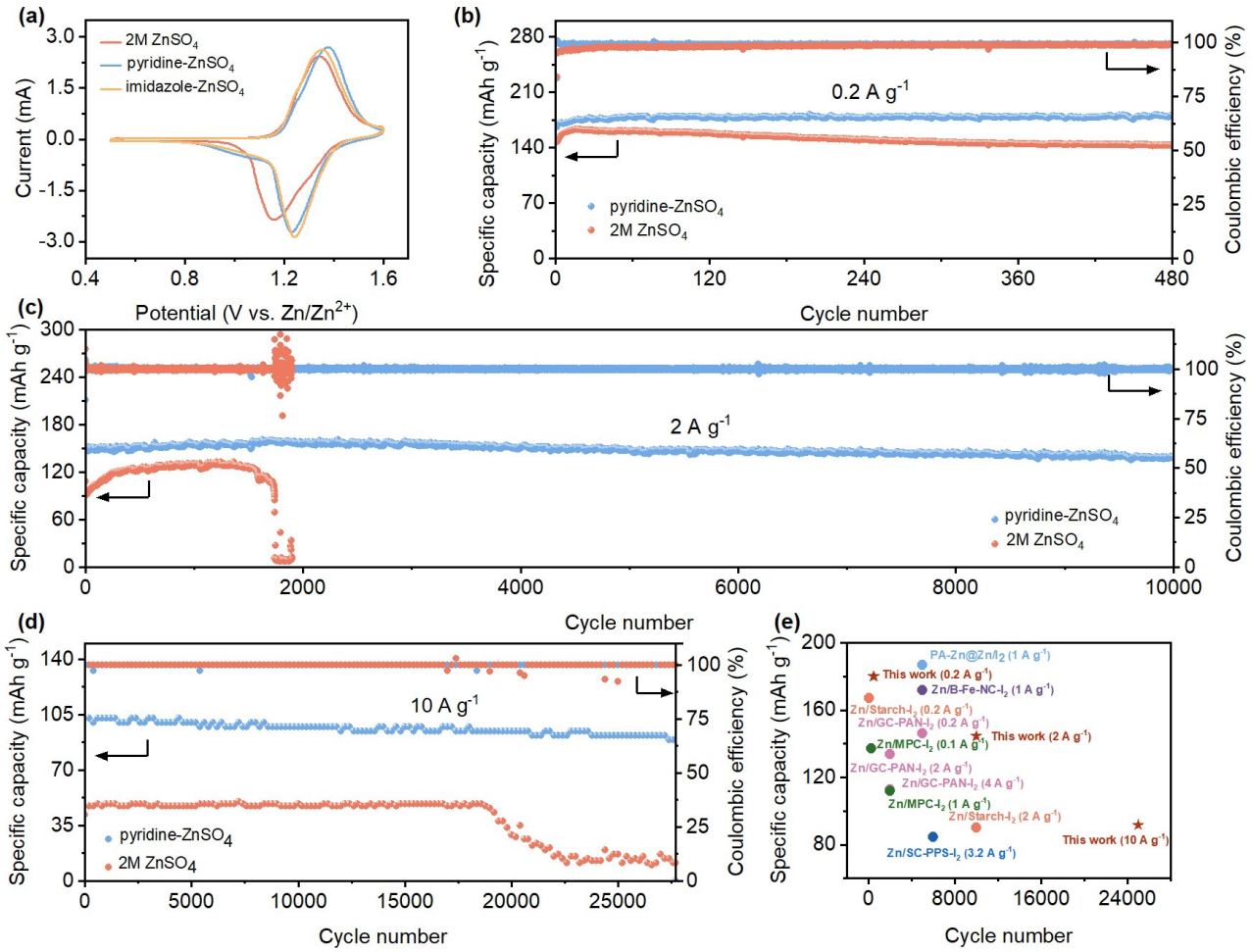

Figure 4. Electrochemical performance for Zn-I_2 full battery in 2 M $ZnSO_4$ and pyridine-$ZnSO_4$. a) Cyclic voltammetry curve for Zn-I_2 full battery. Cycling performance in 2 M $ZnSO_4$ and pyridine-$ZnSO_4$ at, b) 0.2 A g^{-1}, c) 2 A g^{-1} and d) 10 A g^{-1}. e) Comparison of electrochemical performance for Zn-I_2 batteries in this work with reported Zn-I_2 batteries.

capacity decayed to 156.7 mAh g^{-1} following 480 cycles (Figure S14), which was greater than in 2 M $ZnSO_4$ but less than that in pyridine-$ZnSO_4$. The stability of the modified electrolyte in Zn-I_2 battery was determined *via* increasing the current density to 2 A g^{-1}. The initial capacity in 2 M $ZnSO_4$ electrolyte was 95 mAh g^{-1}, which is significantly less than that in pyridine-$ZnSO_4$ of 151 mAh g^{-1}. The specific capacity for Zn-I_2 full battery gradually increased in 2 M $ZnSO_4$ and decreased significantly following 1400 cycles, Figure 4c. In contrast, the Zn-I_2 full battery circulated 10000 cycles in pyridine-$ZnSO_4$ and the capacity decay rate is significantly low with a final capacity retention rate of 92 % (138.8 mAh g^{-1} at 10000 cycles), Figure S15. Under a current density of 2 A g^{-1}, the initial capacity for Zn-I_2 in imidazole-$ZnSO_4$ of 93.5 mAh g^{-1} is similar to that for 2 M $ZnSO_4$, however, it exhibited (Figure S16) a stable cycle performance of >4000 cycles and maintained good charge/discharge in longer cycling (Figure S17). At a greater current density of 10 A g^{-1}, pyridine-$ZnSO_4$ maintained ultra-high initial capacity of 105.5 mAh g^{-1} and exhibited ultra-long cycle performance of >25000 cycles, Figure 4d. The imidazole-$ZnSO_4$ electrolyte exhibited a stable cycle of 25000 with an initial capacity of 50 mAh g^{-1} (Figure S18). This is significantly better than the performance for Zn-I_2 full battery in 2 M $ZnSO_4$ of 43 mAh g^{-1} and 17000 cycles. In comparison with selected, representative reports, the pyridine-$ZnSO_4$ electrolyte-based Zn-I_2 batteries exhibited a superior long-term cycling performance and competitive specific capacity, Figure 4e and Table S3.[3b,16]

A practical obstacle challenge with application of Zn-I_2 battery is the shuttle effect of iodine. During charge I^- is oxidized to I_2 and produces I_3^- intermediate in the cathode. Some I_3^- is attached to the Zn anode leading to oxidation of Zn to Zn^{2+}, resulting in significant Zn corrosion. I_3^- reduced by metal Zn however leads to regeneration of I^- which slows down reoxidation of I^- in the cathode. Shuttle of reciprocating I_3^- accelerate consumption of Zn and reduces cycle life of the battery. When pyridine-$ZnSO_4$ electrolyte was used in the Zn-I_2 full battery, it exhibited greater capacity and longer cycle in pyridine-$ZnSO_4$ compared with 2 M $ZnSO_4$. To explain this finding, *in-situ* UV/Vis was firstly used to determine conversion of polyiodide compounds in battery

© 2023 The Authors. Angewandte Chemie International Edition published by Wiley-VCH GmbH

15213773, 0, Downloaded from https://onlinelibrary.wiley.com/doi/10.1002/anie.202303011 by University of Adelaide Alumni, Wiley Online Library on [26/04/2023]. See the Terms and Conditions (https://onlinelibrary.wiley.com/terms-and-conditions) on Wiley Online Library for rules of use; OA articles are governed by the applicable Creative Commons License

charge and discharge. As seen in Figure 5b, the solubility for I_3^- in 2 M $ZnSO_4$ electrolyte continued to increase with increase in charging time. However, when pyridine was added, the concentration of I_3^- remained at a low concentration, Figure 5a. The concentration of I_3^- was computed in 2 M ZnSO4 and pyridine-$ZnSO_4$, Figure 5c (Figure S19 and Table S4). During 20 min of charging the concentration of I_3^- in pyridine-$ZnSO_4$ increased from 0.095 to 0.121 mM. In contrast, the concentration of I_3^- at the end of 2 M $ZnSO_4$ charging was 0.321 mM, a value significantly greater than the concentration of I_3^- in pyridine-$ZnSO_4$. Figure 5d (and Figure S20) present the *in-situ* Raman spectra for the process of charge and discharge of Zn-I_2 full battery in pyridine-$ZnSO_4$ and 2 M $ZnSO_4$. The I_2/I^- conversion for Zn-I_2 battery in pyridine-$ZnSO_4$ is mainly intermediates I_3^- (110 cm^{-1}) and I_5^- (170 cm^{-1}). As is shown in Figure 5d, the intensity for I_3^- and I_5^- in pyridine-$ZnSO_4$ gradually increased in the initial stage of charging, whilst in the later stage the intensity for Raman peaks of I_3^- and I_5^- gradually decreased until they disappeared. In discharging, the changes in I_3^- and I_5^- exhibit the same trend as for charging. The disappearance of I_3^- and I_5^- Raman peaks following charge and discharge evidence complete conversion of I_2/I^-. However, *via in-situ* Raman the conversion of I_2/I^- in Zn-I_2 battery was evidenced to be mainly intermediates of I_3^- in 2 M $ZnSO_4$ and Raman peak intensity for I_5^- was low (Figure S20), and following charge/discharge I_3^- was still present. Dominant I_3^- leads to incomplete conversion of I_2/I^- in 2 M $ZnSO_4$, and finally to continuous attenuation of capacity of Zn-I_2 battery and short cycle life. To determine conversion of I_3^- and I_5^- in the electrolyte, the Enthalpy (H) for iodine reduction in 2 M $ZnSO_4$ and pyridine-$ZnSO_4$ was computed, Figure 5e. In 2 M $ZnSO_4$ electrolyte the ΔH decreases for $*I_2$ to $*I_3$ and then to $*I_5$, evidencing spontaneous behaviour of the conversion from $*I_2$ to $*I_3$ (−0.17 eV) and then to $*I_5$ (−0.53 eV). This allows significant $*I_3$ and $*I_5$ to exist throughout the I_2/I^- conversion, resulting in an incomplete conversion of I_2/I^-. Therefore, a small amount of I_3^- remains in 2 M $ZnSO_4$ following the first charge and discharge (Figure S20) that is in agreement with *in-situ* Raman findings. In pyridine-$ZnSO_4$ electrolyte however, the conversion of $*I_2$ to $*I_3$ (+0.47 eV) is inhibited, whilst conversion of $*I_2$ to $*I_5$ (+0.1 eV) is favourable, contributing to the relatively high concentration of $*I_5$ in pyridine-$ZnSO_4$ electrolyte compared to that for $*I_3$. This is likely the reason for the stronger peak for $*I_5$ than $*I_3$ in the Raman spectra, and lower concentration of $*I_3$ in UV/Vis spectra for pyridine-$ZnSO_4$ electrolyte. The adsorption energy for $*I_2$ in pyridine and $ZnSO_4$ were computed (Figure S21). Pyridine exhibited stronger interactions as evidenced by a more negative adsorption energy, facilitating reduction of I_2 into $*I^-$. It is concluded therefore that combined experiment and theoretical computation confirm the pyridine additive suppresses formation of intermediate (I_3^-) and reduces conversion barriers for I_2/I^-, and boosts reversibility and stability of Zn-I_2 batteries.

The overall mechanism for organic pH buffer additive in Zn-I_2 full battery, based on the experimental and theoretical evidence, is presented as Figure 6. The Zn-I_2 battery in conventional $ZnSO_4$ electrolyte exhibits the following drawbacks, 1) A significant number of active H_2O molecules in electrolyte will be electrolysed to H^+ and OH^-, and

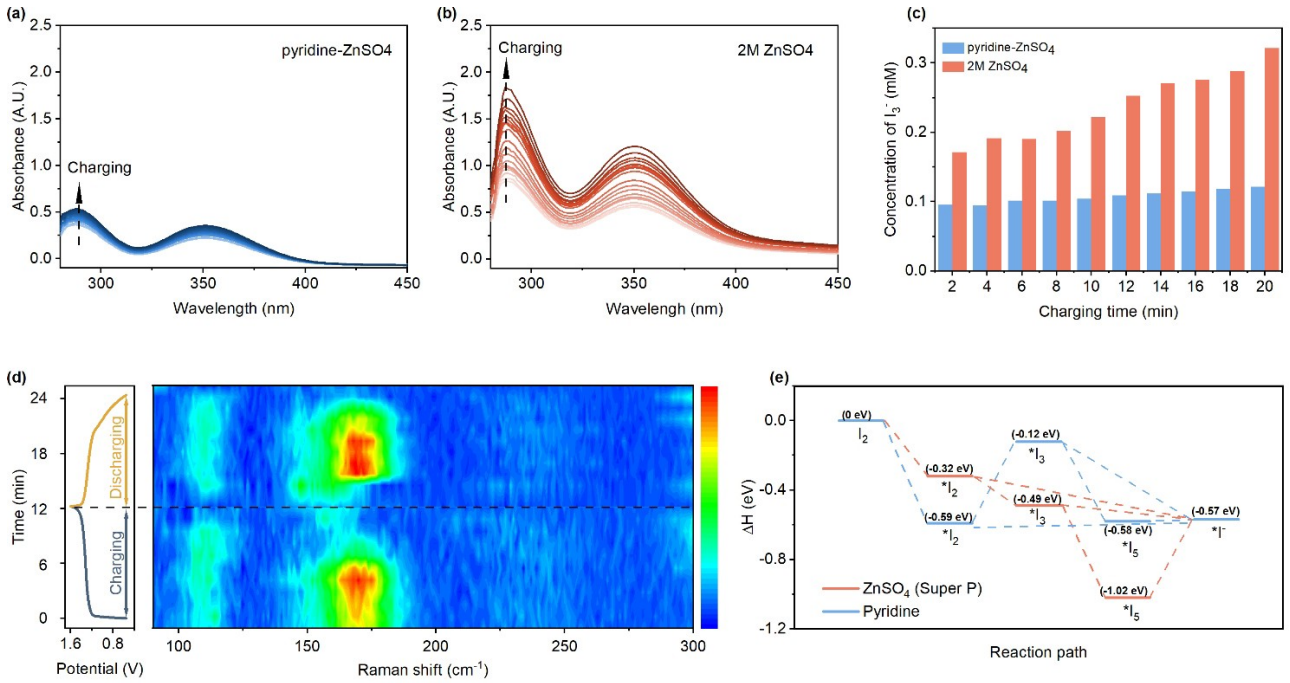

Figure 5. Shuttle suppression mechanism in Zn-I_2 battery. a), b) *In-situ* UV/Vis spectra for pyridine-$ZnSO_4$ and 2 M $ZnSO_4$ during charge. c) Evolution of I_3^- concentration from *in-situ* UV/Vis in pyridine-$ZnSO_4$ and 2 M $ZnSO_4$. d) *In-situ* Raman showing charge/discharge of I^-/I_2 conversion in pyridine-$ZnSO_4$. e) Enthalpy diagram for I_2 reduction in pyridine-$ZnSO_4$ and $ZnSO_4$ (Super P), where * represents active site.

© 2023 The Authors. Angewandte Chemie International Edition published by Wiley-VCH GmbH

15213773, 0, Downloaded from https://onlinelibrary.wiley.com/doi/10.1002/anie.202303011 by University of Adelaide Alumni, Wiley Online Library on [26/04/2023]. See the Terms and Conditions (https://onlinelibrary.wiley.com/terms-and-conditions) on Wiley Online Library for rules of use; OA articles are governed by the applicable Creative Commons License

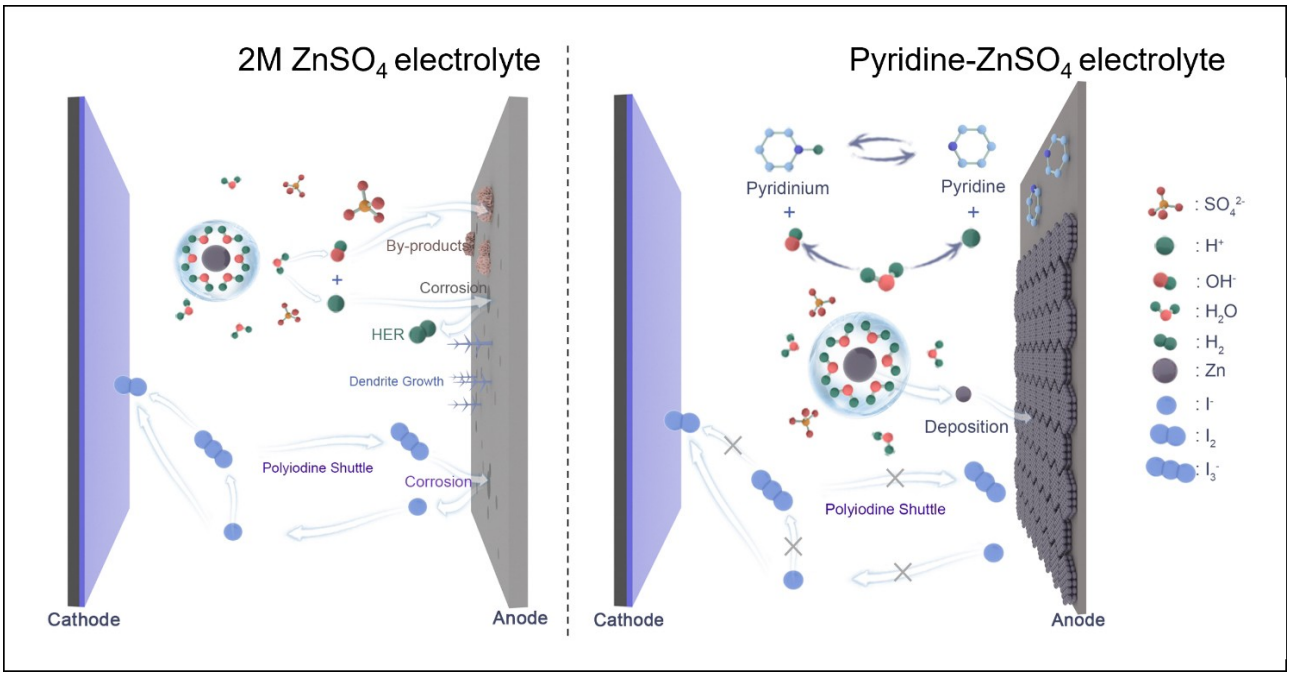

Figure 6. Schematic for mechanism for Zn-I_2 full battery. For, left to right, respectively, 2 M $ZnSO_4$ and pyridine-$ZnSO_4$ electrolyte.

accumulated H^+ will obtain electrons in discharge and reduce to H_2 resulting in corrosion of Zn anode, 2) The release of H_2 leads to gradual increase in OH^- concentration, and readily produces Zn_xSO_y $(OH)_z{\cdot}nH_2O$ by-products passivating the Zn anode and impacting CE, 3) The uncontrolled deposition of Zn is accompanied by production of Zn anode by-products that leads to dendritic growth, and; 4) The presence of high concentration of polyiodine compounds diffuses to Zn anode through concentration difference resulting in self-discharge, and to corrosion of Zn anode ($I_3^- + 2e^- \rightarrow 3I^-$, $Zn\text{-}2e^- \rightarrow Zn^{2+}$). Concurrently, in the reaction I^- generated *via* self-discharge with Zn reacts with I_2 to form I_3^- ($I_2 + I^- \rightarrow I_3^-$) that consumes more I_2, and leads to decline in CE and capacity of the full Zn-I_2 battery. However, in using a pH buffer solution containing N heterocyclic compound pyridine and imidazole, H^+ are bound by N that inhibits reduction of H_2. With the concentration of OH^- continuing to rise the bound H^+ combines with OH^- to reduce the fluctuation of pH. Additionally, pyridine and imidazole preferentially absorb on Zn metal surface to suppress dendritic growth and induce uniform deposition of Zn, especially the pyridine additive dominated by surface energy that induces stacking deposition of Zn at (002) facet. Pyridine-$ZnSO_4$ inhibits the conversion of polyiodine compounds and reduces the conversion barrier for I/I^- in Zn-I_2 full battery. The high enthalpy for I_3^- makes it difficult for I_2 to form I_3^- in pyridine-$ZnSO_4$ electrolyte. This inhibits the generation of polyiodine compounds preventing the diffusion of high concentration polyiodine compounds to Zn anode, thereby promoting full conversion of I_2/I^-, and reducing consumption of I_2 and inhibiting corrosion of Zn anode. The result is high capacity and long-life operation of Zn-I_2 full batteries.

Conclusion

A new organic pH buffer containing N heterocyclic compounds can be practically used as an additive to regulate pH in conventional $ZnSO_4$ electrolyte. *In-situ* pH and *in-situ* GC confirm that pyridine and imidazole inhibit H_2 evolution and maintain stability of pH. The inhibition of H_2 significantly reduces passivation of Zn anode and boosts reversibility of Zn. Importantly, pyridine and imidazole preferentially absorb on the Zn metal surface to result in a uniform, dendrite-free deposition of Zn. Zn/Zn symmetric batteries in pyridine-$ZnSO_4$ and imidazole-$ZnSO_4$ therefore exhibit excellent reversibility and stability. In particular, a Zn/Zn symmetric battery in pyridine-$ZnSO_4$ exhibited a stable cycle of 3200 h at 2 mA cm^{-2} and 2 mAh cm^{-2}, and a cycle of 600 h at a high current density and capacity of 5 mA cm^{-2} and 5 mAh cm^{-2}. Significantly, pyridine and imidazole also suppress the formation of polyiodine intermediates. The Zn-I_2 full batteries in pyridine-$ZnSO_4$ and imidazole-$ZnSO_4$ therefore exhibited greater cycle stability and greater capacity than that in 2 M $ZnSO_4$. We conclude that targeted engineering of electrolyte pH using organic buffer additive is of benefit in practical design for highly reversible and dendrite-free and shuttle-free Zn-I_2 batteries, and therefore of interest to researchers and manufacturers.

Acknowledgements

Financial support provided by the Australian Research Council (ARC) Discovery Projects (DP200101862, FL210100050) is gratefully acknowledged. Open Access publishing facilitated by The University of Adelaide, as part

© 2023 The Authors. Angewandte Chemie International Edition published by Wiley-VCH GmbH

15213773, 0, Downloaded from https://onlinelibrary.wiley.com/doi/10.1002/anie.202303011 by University of Adelaide Alumni, Wiley Online Library on [26/04/2023]. See the Terms and Conditions (https://onlinelibrary.wiley.com/terms-and-conditions) on Wiley Online Library for rules of use; OA articles are governed by the applicable Creative Commons License

of the Wiley - The University of Adelaide agreement via the Council of Australian University Librarians.

Conflict of Interest

The authors declare no conflict of interest.

Data Availability Statement

The data that support the findings of this study are available from the corresponding author upon reasonable request.

Keywords: Electrolyte Additives · Organic pH Buffer · Zn Metal · Zn–Iodine Batteries

[1] a) Y. Y. Wang, Z. J. Wang, F. H. Yang, S. L. Liu, S. L. Zhang, J. F. Mao, Z. P. Guo, *Small* **2022**, *18*, 2107033; b) S. L. Zhang, Y. Liu, Q. N. Fan, C. F. Zhang, T. F. Zhou, K. Kalantar-Zadeh, Z. P. Guo, *Energy Environ. Sci.* **2021**, *14*, 4177–4202; c) J. F. Mao, C. Ye, S. L. Zhang, F. X. Xie, R. Zeng, K. Davey, Z. P. Guo, S. Z. Qiao, *Energy Environ. Sci.* **2022**, *15*, 2732–2752; d) Z. J. Wang, Y. Y. Wang, B. H. Li, J. C. Bouwer, K. Davey, J. Lu, Z. P. Guo, *Angew. Chem. Int. Ed.* **2022**, *61*, e202206682; e) M. N. Li, C. Y. Wang, K. Davey, J. X. Li, G. J. Li, S. L. Zhang, J. F. Mao, Z. P. Guo, *SmartMat* **2023**, https://doi.org/10.1002/smm2.1185.

[2] a) H. J. Huang, D. M. Xie, J. C. Zhao, P. H. Rao, W. M. Choi, K. Davey, J. F. Mao, *Adv. Energy Mater.* **2022**, *12*, 2202419; b) S. Liu, J. Vongsvivut, Y. Wang, R. Zhang, F. Yang, S. Zhang, K. Davey, J. Mao, Z. Guo, *Angew. Chem. Int. Ed.* **2023**, *62*, e202215600.

[3] a) S. L. Liu, R. Z. Zhang, J. F. Mao, Y. L. Zhao, Q. Cai, Z. P. Guo, *Sci. Adv.* **2022**, *8*, eabn5097; b) S. J. Zhang, J. N. Hao, H. Li, P. F. Zhang, Z. W. Yin, Y. Y. Li, B. K. Zhang, Z. Lin, S. Z. Qiao, *Adv. Mater.* **2022**, *34*, 2201716.

[4] a) X. S. Zhao, X. Zhang, N. Dong, M. D. Yan, F. L. Zhang, K. Mochizuki, H. L. Pan, *Small* **2022**, *18*, 2200742; b) Y. Q. Lv, Y. Xiao, L. T. Ma, C. Y. Zhi, S. M. Chen, *Adv. Mater.* **2022**, *34*, 2106409; c) L. S. Cao, D. Li, E. Y. Hu, J. J. Xu, T. Deng, L. Ma, Y. Wang, X. Q. Yang, C. S. Wang, *J. Am. Chem. Soc.* **2020**, *142*, 21404–21409; d) S. L. Liu, J. F. Mao, W. K. Pang, J. Vongsvivut, X. H. Zeng, L. Thomsen, Y. Y. Wang, J. W. Liu, D. Li, Z. P. Guo, *Adv. Funct. Mater.* **2021**, *31*, 2104281; e) M. D. Yan, N. Dong, X. S. Zhao, Y. Sun, H. L. Pan, *ACS Energy Lett.* **2021**, *6*, 3236–3243.

[5] a) D. Xie, Y. Sang, D. H. Wang, W. Y. Diao, F. Y. Tao, C. Liu, J. W. Wang, H. Z. Sun, J. P. Zhang, X. L. Wu, *Angew. Chem. Int. Ed.* **2023**, *62*, e202216934; b) W. Zhang, Y. H. Dai, R. W. Chen, Z. M. Xu, J. W. Li, W. Zong, H. X. Li, Z. Li, Z. Y. Zhang, J. X. Zhu, F. Guo, X. Gao, Z. J. Du, J. T. Chen, T. L. Wang, G. J. He, I. P. Parkin, *Angew. Chem. Int. Ed.* **2023**, *62*, e202212695; c) F. Wang, O. Borodin, T. Gao, X. L. Fan, W. Sun, F. D. Han, A. Faraone, J. A. Dura, K. Xu, C. S. Wang, *Nat. Mater.* **2018**, *17*, 543–549; d) C. Zhang, J. Holoubek, X. Y. Wu, A. Daniyar, L. D. Zhu, C. Chen, D. P. Leonard, I. A. Rodriguez-Perez, J. X. Jiang, C. Fang, X. Ji, *Chem. Commun.* **2018**, *54*, 14097–14099; e) L. Zhang, I. A. Rodriguez-Perez, H. Jiang, C. Zhang, D. P. Leonard, Q. B. Guo, W. F. Wang, S. M. Han, L. M. Wang, X. L. Ji, *Adv. Funct. Mater.* **2019**, *29*, 1902653; f) J. H. Liu, Z. Khanam, S. Ahmed, T. Wang, H. T. Wang, S. H. Song, *ACS Appl. Mater. Interfaces* **2021**, *13*, 16454–16468; g) F. N. Mo, G. J. Liang, Q. Q. Meng, Z. X. Liu, H. F. Li, J. Fan, C. Y. Zhi, *Energy Environ. Sci.* **2019**, *12*, 706–715; h) S. L. Zhang, N. S. Yu, S. Zeng, S. S. Zhou, M. H. Chen, J. T. Di, Q. W. Li, *J. Mater. Chem. A* **2018**, *6*, 12237–12243; i) W. Kao-ian, M. T. Nguyen, T. Yonezawa, R. Pornprasertsuk, J. Qin, S. Siwamogsatham, S. Kheawhom, *Mater. Today* **2021**, *21*, 100738; j) J. N. Hao, L. B. Yuan, C. Ye, D. L. Chao, K. Davey, Z. P. Guo, S. Z. Qiao, *Angew. Chem. Int. Ed.* **2021**, *60*, 7366–7375.

[6] B. Li, Z. M. Nie, M. Vijayakumar, G. S. Li, J. Liu, V. Sprenkle, W. Wang, *Nat. Commun.* **2015**, *6*, 6303.

[7] a) Y. Q. Yang, S. Q. Liang, B. A. Lu, J. Zhou, *Energy Environ. Sci.* **2022**, *15*, 1192–1200; b) X. H. Zeng, K. X. Xie, S. L. Liu, S. L. Zhang, J. N. Hao, J. T. Liu, W. K. Pang, J. W. Liu, P. H. Rao, Q. H. Wang, J. F. Mao, Z. P. Guo, *Energy Environ. Sci.* **2021**, *14*, 5947–5957.

[8] M. I. Zaki, M. A. Hasan, F. A. Al-Sagheer, L. Pasupulety, *Colloids Surf. A* **2001**, *190*, 261–274.

[9] a) M. Mohsen, I. Naeem, M. Awaad, H. Tantawy, A. Baraka, *J. Solid State Chem.* **2020**, *289*, 121493; b) T. Rajkumar, G. R. Rao, *Mater. Chem. Phys.* **2008**, *112*, 853–857.

[10] X. H. Zeng, J. T. Liu, J. F. Mao, J. N. Hao, Z. J. Wang, S. Zhou, C. D. Ling, Z. P. Guo, *Adv. Energy Mater.* **2020**, *10*, 1904163.

[11] F. Yang, J. A. Yuwono, J. Hao, J. Long, L. Yuan, Y. Wang, S. Liu, Y. Fan, S. Zhao, K. Davey, *Adv. Mater.* **2022**, *34*, 2206754.

[12] Z. M. Zhao, J. W. Zhao, Z. L. Hu, J. D. Li, J. J. Li, Y. J. Zhang, C. Wang, G. L. Cui, *Energy Environ. Sci.* **2019**, *12*, 1938–1949.

[13] Z. D. Zhao, R. Wang, C. X. Peng, W. J. Chen, T. Q. Wu, B. Hu, W. J. Weng, Y. Yao, J. X. Zeng, Z. H. Chen, P. Y. Liu, Y. C. Liu, G. S. Li, J. Guo, H. B. Lu, Z. P. Guo, *Nat. Commun.* **2021**, *12*, 6606.

[14] P. Sun, L. Ma, W. H. Zhou, M. J. Qiu, Z. L. Wang, D. L. Chao, W. J. Mai, *Angew. Chem. Int. Ed.* **2021**, *60*, 18247–18255.

[15] C. B. Deng, X. S. Xie, J. W. Han, Y. Tang, J. W. Gao, C. X. Liu, X. D. Shi, J. Zhou, S. Q. Liang, *Adv. Funct. Mater.* **2020**, *30*, 2000599.

[16] a) L. Q. Zhang, M. J. Zhang, H. L. Guo, Z. H. Tian, L. F. Ge, G. J. He, J. J. Huang, J. T. Wang, T. X. Liu, I. P. Parkin, F. L. Lai, *Adv. Sci.* **2022**, *9*, 2105598; b) Y. Z. Hou, F. G. Kong, Z. R. Wang, M. M. Ren, C. D. Qiao, W. L. Liu, J. S. Yao, C. B. Zhang, H. Zhao, *J. Colloid Interface Sci.* **2023**, *629*, 279–287; c) L. Q. Zhang, J. J. Huang, H. L. Guo, L. F. Ge, Z. H. Tian, M. J. Zhang, J. T. Wang, G. J. He, T. X. Liu, J. Hofkens, D. J. L. Brett, F. L. Lai, *Adv. Energy Mater.* **2023**, *13*, 2203790; d) M. M. Liu, Q. W. Chen, X. Y. Cao, D. X. Tan, J. Z. Ma, J. T. Zhang, *J. Am. Chem. Soc.* **2022**, *144*, 21683–21691; e) S. Chen, Q. W. Chen, J. Z. Ma, J. J. Wang, K. S. Hui, J. T. Zhang, *Small* **2022**, *18*, 2200168.

Manuscript received: February 28, 2023
Accepted manuscript online: March 22, 2023
Version of record online: ■■, ■■

© 2023 The Authors. Angewandte Chemie International Edition published by Wiley-VCH GmbH

15213773, 0, Downloaded from https://onlinelibrary.wiley.com/doi/10.1002/anie.202303011 by University of Adelaide Alumni, Wiley Online Library on [26/04/2023]. See the Terms and Conditions (https://onlinelibrary.wiley.com/terms-and-conditions) on Wiley Online Library for rules of use; OA articles are governed by the applicable Creative Commons License

Research Articles

$Zn\text{-}I_2$ Batteries

Y. Lyu, J. A. Yuwono, P. Wang, Y. Wang, F. Yang, S. Liu, S. Zhang, B. Wang, K. Davey, J. Mao,* Z. Guo* _ **e202303011**

Organic pH Buffer for Dendrite-Free and Shuttle-Free $Zn\text{-}I_2$ Batteries

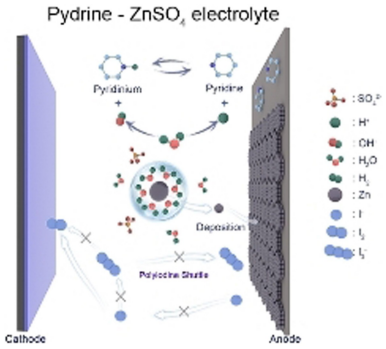

An organic pH buffer strategy is proposed. N-containing organic molecules simultaneously control electrolyte pH, suppress hydrogen evolution, enable uniform Zn deposition, and inhibit shuttle of polyiodine compounds, achieving highly reversible and stable, long-cycle $Zn\text{-}I_2$ batteries.

© 2023 The Authors. Angewandte Chemie International Edition published by Wiley-VCH GmbH

15213773, 0, Downloaded from https://onlinelibrary.wiley.com/doi/10.1002/anie.202303011 by University of Adelaide Alumni, Wiley Online Library on [26/04/2023]. See the Terms and Conditions (https://onlinelibrary.wiley.com/terms-and-conditions) on Wiley Online Library for rules of use; OA articles are governed by the applicable Creative Commons License